Journal of Materials Chemistry A

Accepted Manuscript

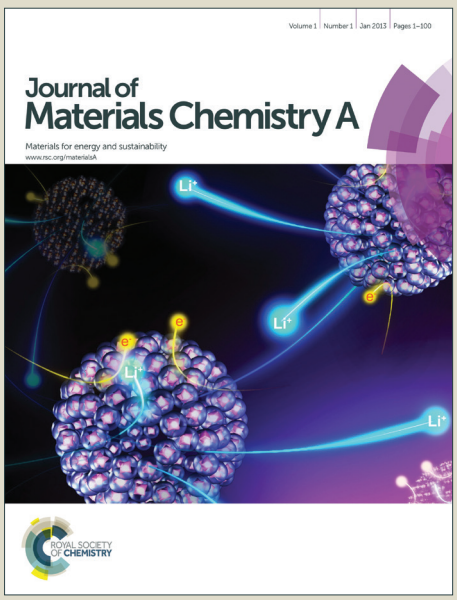

ROYAL SOCIETY OF CHEMISTRY

www.rsc.org/materialsA

Fabrication of ultralight three-dimensional graphene networks with strong electromagnetic wave absorption properties

Weiwei Liu,† Hua Li†*, Qingping Zeng, Huanan Duan, Yiping Guo, Xuefa Liu, Chongyang Sun, Hezhou Liu*

State Key Laboratory of Metal Matrix Composites, School of Materials Science and Engineering, Shanghai Jiao Tong University, Shanghai 200240, People's Republic of China

Corresponding author: Hua Li, lih@sjtu.edu.cn ;

Hezhou Liu, hzhliu@sjtu.edu.cn.

Tel.: +86 021 34202549.

Postal Address: Room 331, Material Building D, Shanghai JiaoTong University, Dongchuan Road No. 800, Minhang District, Shanghai, 200240, The People's Republic of China.

† W. W. Liu and H. Li contributed equally to this work.

ABSTRACT

Thermally reduced graphene networks (TRGN) with low densities less than 10 mg cm^{-3} were synthesized by thermal reduction of graphene oxide/poly(vinyl alcohol) networks. To evaluate the electromagnetic wave absorption properties of TRGN, TRGN were nondestructively backfilled with wax via a vacuum-assisted method. The as-prepared TRGN/wax composites using integrated TRGN as fillers rather than directly dispersing graphene sheets in wax exhibit better electromagnetic wave absorption capabilities due to the 3D conductive frameworks, which could generate more effective electrical loss in terms of dissipating the induced current in the TRGN/wax composites. Specifically, for the TRGN/wax composite with ~1 wt% TRGN, the minimum reflection loss reaches -43.5 dB at 12.19 GHz with a thickness of 3.5 mm and the bandwidth of reflection loss less than -10 dB (90% absorption) can reach up to 7.47 GHz. More importantly, our work provides a promising approach to construct graphene-based composites with strong electromagnetic wave absorption ability at very low filler loadings.

1. Introduction

With the rapid development of electronic devices and communication facilities, severe electromagnetic (EM) radiation has become a pollution problem, which is harmful to both highly sensitive precision electronic equipment and the health of human beings.[1, 2] To date, the EM wave absorbers with strong absorption abilities and the lightweight characteristics have been greatly requested. Therefore, EM wave absorbing materials have attracted increasing attention and EM absorption properties of various nanostructures have been widely investigated.[3-12] Compared to other kinds of EM absorbing materials, carbon based materials exhibit many excellent properties, including good corrosion resistance, light weight, a wide absorption frequency and high thermal stability.[13-15] As a new kind of carbon material, graphene, a two-dimensional (2D) sheet composed of sp^2-bonded carbon atoms, has drawn significant attention due to its extraordinary electrical, thermal, mechanical properties and high specific surface area.[16] The surface area of graphene can reach up to above 1000 $m^2 g^{-1}$, which indicates that it can be applied as a lightweight EM absorber. However, good electrical conductivity is harmful for EM wave absorption according to the impedance mechanism. Due to the high conductivity, graphene has a strong dielectric loss, but a weak attenuation to EM wave.[17-19] The related materials of graphene, such as graphene oxide (GO) and reduced graphene oxide (RGO), have been widely investigated due to their scalability, high yield, and the easiness of functionalization. GO can be reduced into RGO by chemical,[20] thermal,[21] and electrochemical[22] reduction. The conductivity of RGO is much lower than graphene due to the defects and functional groups introduced into RGO during the wet chemical and thermal treatment processes. Thus many researchers chose RGO to fabricate EM wave absorbing materials. Wang and coworkers, who studied the EM property of

chemically reduced graphene oxide (RGO), demonstrated that RGO showed enhanced EM wave absorption compared with graphite and carbon nanotubes, and the dielectric loss was the main EM wave absorbing mechanism of RGO.[17] Bai et al. prepared RGO/poly(ethylene oxide) composites with 5 wt% RGO, and the reflection loss (RL) could reach -38.8 dB with the effective bandwidth (below -10 dB) ranging from 13.9 to 18 GHz.[23] Singh et al. fabricated RGO/nitrile butadiene rubber composites with 10 wt% RGO which had a maximum absorption value of -57 dB and a wide effective bandwidth from 7.5 to 12 GHz.[24] Guo et al. investigated the EM wave absorption properties of PVDF/RGO composites with 1 wt%, 3 wt% and 7 wt% RGO in the frequency range of 2-18 GHz, and the RL of the composite with a low filler loading of 3 wt% could reach -25.6 dB at 10.8 GHz.[25]

In addition to bare RGO fillers, researchers have also studied the EM wave absorption properties of the hybrid structures. Sun et al. synthesized the Fe_3O_4/RGO hybrids, and their wax-based composites with 40 wt% filler loading which exhibited a maximum absorption of -26.4 dB with an effective bandwidth of 2 GHz from 4.5 to 6.5 GHz.[4] Chen et al. reported that the composites with 60 wt% RGO/Ni hybrids presented a minimum reflection loss of -17 dB with effective bandwidth ranges of 3-4 GHz and 12-14 GHz.[26] Recently, Cao et al. synthesized $MnFe_2O_4$ nanoparticles and reported that the RGO/$MnFe_2O_4$/PVDF composite at a very low filler loading of 5 wt% attained a RL below -10 dB from 8.00 to 12.88 GHz, and a minimum RL of -29.0 dB at 9.2 GHz.[27] However, the filler loadings of most reported hybrids-based composites are still very high, which will limit the application of the hybrid structures in producing lightweight EM wave absorbing composites. It is found that the composites with bare carbon fillers require much lower filler loadings to reach the targeting performance when compared with hybrid structures.[28-31] Nevertheless, all these

researches were confined to study the EM wave absorption properties of 2D graphene and 2D graphene composites. What is more, the application of these new carbon materials are always limited by problems of poor dispersion, high interfacial contact electrical resistance between carbon fillers and the complex permittivity deviating from the optimal values when used as EM wave absorbing materials.[32]

3D graphene structures have some unique characteristics such as low density, high porosity, large specific surface area and good electrical conductivity.[33-37] Zhang et al. fabricated macroscopic RGO-α-Fe_2O_3 and RGO-Fe_3O_4 hydrogels with 3D interconnected networks, and the composites prepared by uniformly mixing 8 wt% of the hydrogels with paraffin matrix presented good EM wave absorption properties. The effective bandwidth of these two composites were 7.12 GHz and 5.3 GHz, and the minimum RL of them were -33.5 dB and -47.9 dB, respectively.[38, 39] Hence, 3D graphene networks are promising candidates for the construction of lightweight EM wave absorbing materials if their 3D structures can be retained.

Unlike other reports, in this paper, the vacuum-assisted infusion technique was employed to transfer wax into 3D graphene networks to avoid damaging the 3D structure instead of mixing fillers in matrix. 3D graphene networks were used as absorbers for EM wave. The 3D conductive graphene frameworks play a significant role in the dissipation of the electrical current induced by the EM wave. Therefore, highly effective EM wave absorption at very low filler loading could be achieved successfully in this way.

2. Experimental

2.1 Material preparation

GO was prepared from natural graphite flake by a modified Hummers method.[24] PVA was purchased from Aladdin Reagent Co. and used as received. Concentrated sulfuric acid (H_2SO_4), potassium permanganate ($KMnO_4$), sodium nitrate ($NaNO_3$), hydrochloric acid (HCl) were purchased from Sinopharm Chemical Reagents Company and used directly without further purification.

2.2 Fabrication of 3D graphene network

GO contains many oxygen-containing functional groups therefore it can be dispersed very well at the level of individual sheet in water.[40] PVA is also water-soluble due to plenty of hydroxyl groups. In addition, potential H-bonding between GO and PVA could result in enhanced interfacial adhesion. Therefore, PVA is expected to have truly homogenous co-dispersion with GO at the molecular level.[41, 42] GO/PVA solution was prepared through a solution-mixing method. Typically, GO (60 mg) was dispersed in water (20 ml) in an ultrasonic bath for 1 h at 25 ℃ to yield a clear solution, and then PVA (0.2 g) was added to the GO solution under vigorous stirring for 1h. The as-prepared gel was freeze-dried for 48 h to obtain the graphene oxide network, which was further annealed in a quartz tube by an alcohol blast burner (about 800 ℃)[43] under nitrogen atmosphere for 10 min. Upon drying and annealing, PVA, which connected GO sheets, was pyrolyzed. Due to the pyrolysis of PVA, the size of TRGN will be a little smaller than the GO/PVA network. The as-synthesized 3D graphene network was denoted as TRGN-1 hereafter. Three other TRGN were synthesized with different amounts (140 mg, 220 mg and 300 mg) of GO following the same procedure, and they were named as TRGN-2, TRGN-3 and TRGN-4, and their densities were calculated to be 4.1 mg cm^{-3}, 8.1 mg cm^{-3}, 12.4mg cm^{-3} and 16.3 mg cm^{-3}, respectively.

2.3 Preparation of 3D graphene network/wax composites

The 3D graphene network/wax composites were prepared by the vacuum-assisted impregnation. The formation process of TRGN/wax composite was shown in Fig. 1 .In the impregnation method, paraffin wax was heated to 80 ℃ to melt, and the TRGN were completely immersed into the melted wax. Then the mixtures were placed in a vacuum oven for 15 min for the TRGN to be backfilled with the wax and to remove air bubbles. Finally, the 3D graphene network/wax composites were cooled down at room temperature for 4 h, and excessive wax adhered on the TRGN surface was removed. The graphene loading in the composites was calculated by measuring the weight of TRGN before and after the wax impregnation. The graphene loadings of the composites with TRGN-1 , TRGN-2, TRGN-3 and TRGN-4 were calculated to be ~0.5 wt% and ~1 wt%, ~1.5 wt% and ~2.0 wt%, respectively.

2.4 Characterizations

The XRD spectra were acquired by D/MAX2550/PC using Cu Kα radiation from 8 °to 50 ° at a scan rate of 10 ° min^{-1} under 35 kV and 200 mA. Scanning electronic microscopy (SEM) images were obtained on a Hitachi S-4800 field-emission SEM operated at 10 kV. Raman spectra were taken on a SENTERRA R200 Raman spectrometer with a 633 nm laser excitation. X-ray photoelectron spectroscopy (XPS) was recorded using a Kratos Axis Ultra DLD spectrometer. The conductivity of these as-prepared TRGN was measured by the four-point method using a four-probe conductivity measurement device (RST-8, Guangzhou, China). The pyrolysis processes of PVA and GO/PVA network were studied using the thermogravimetric analysis (TGA) method under nitrogen atmosphere at a heating rate of 10 ℃ min^{-1} (STA449F3, Netzsch, Germany).The composite samples used for EM wave

absorption measurement were prepared using two punchers (one with an inner diameter of 7.00 mm and the other one with an outer diameter of 3.04 mm) to get toroidal shaped samples (φ_{out} , 7.00 mm; φ_{in}, 3.04 mm). In this way, the 3D graphene structures in the composites were well remained. The TRGN-1, TRGN-2, TRGN-3 and TRGN-4/wax composite were respectively named as S1-1, S2-1, S3-1 and S4-1. Controlled experiment was also conducted using composites which were made by uniformly mixing 0.5 wt% of smashed TRGN-1 , 1 wt% of smashed TRGN-2, 1.5 wt% of smashed TRGN-3 and 2 wt % of smashed TRGN-4 with wax. Afterward, the mixtures were pressed into toroidal shape (φ_{out}, 7.00 mm; φ_{in}, 3.04 mm). The sample with 0.5 wt% of smashed TRGN-1 was named as S1-2, and the other corresponding samples were named as S2-2, S3-2 and S4-2. The complex permittivity values were measured using an Agilent 85050D vector network analyzer in the frequency range of 2-18 GHz. Considering no ferromagnetic materials were involved in our experiments, complex permeability was taken as 1 (u_r =1).

3. Results and discussion

The reduction process could be proved by XRD patterns, Raman spectra and XPS. As shown in Fig.2a, the XRD pattern of GO exhibits a feature diffraction peak at ~10.5 °. In the case of TRGN-1, this peak is disappeared and a relatively broad peak at ~25 ° is observed, which means that the GO has been transformed to reduced graphene with significantly less functionalities.[20, 44] The Raman spectra of GO and TRGN-1 are compared in Fig.2b. The peak centered at 1346 cm^{-1} is assigned to D band which is associated with the structural imperfections caused by the defects and presence of functional groups. The peak located at 1576 cm^{-1} is attributed to G band which is the characteristic of the sp^2-hybridized carbon-carbon bonds.[45] The peak area ratio of the D band to G band for TRGN-1 was increased from 1.58 to 1.82 when compared with

that of GO. The increase in the ratio of the A(D)/A(G) can be attributed to an increase in the quantity of amorphous carbon, a higher density of defects on the structure, or a reduction in the crystallite size or domains.[46]

Fig. 3a shows the TGA of PVA, it is found that when the temperature is higher than 700 ℃, nearly 99% wt% PVA will be burnt out. Fig. 3b displays that the weight loss of GO/PVA network can reach 74.6% when the temperature is 700 ℃, which means more than 97 wt% PVA could be pyrolyzed and only about 3 wt% PVA could be changed to carbon under the alcohol blast burner in nitrogen atmosphere. Thus, TRGN would be primarily made up of reduced graphene and could be very light. After thermal reduction, the TRGN are conductive, and the conductivities of TRGN-1, TRGN-2, TRGN-3 and TRGN-4 are 2.4 S/m, 3.1 S/m, 4.2 S/m, 5.1 S/m, respectively. The conductivity increases with the increased concentration of RGO. The C1s spectrum of GO is presented in Fig.4a, in which four different peaks centered at 284.6, 286.7, 287.9 and 288.8 eV corresponding to C=C/C-C in aromatic rings, C-O (epoxy and alkoxy), C=O(carbonyl) and O-C=O(carboxyl groups), respectively, are observed. However, in TRGN-1, the intensity of the peaks corresponding to oxygen-containing groups decreases dramatically (Fig. 4b) indicating considerable degree of reduction.[34]

SEM images of TRGN-1 are shown in Fig. 5. It can be seen from Fig. 5a and b that TRGN-1 has an interconnected 3D porous network with randomly oriented wrinkled sheet-like structures. The network is composed of large numbers of micrometer-sized pores which endow it with an ultralow density. Fig. 5c-e exhibit the burning process of TRGN-1/wax composite. After the wax was burnt out, the network still remains its 3D porous structure (Fig. 5f). It can be concluded that, with vacuum-assisted impregnation method, the graphene network could remain its original 3D structure when TRGN was backfilled with wax. The photo images and

SEM images of S1-1 and S1-2 are presented in Fig. 6. It is clearly found that the graphene network well retains the 3D architecture in the wax, and the sizes of pores are similar to TRGN-1(Fig. 6a), while the structure of S1-2 is quite different from that of S1-1, conductive interconnections like S1-1 could not be established in S1-2. Therefore, the unique lightweight conductive 3D network should be an ideal material for EM attenuation.

To reveal the EM wave absorbing properties of these as-prepared composites, their real part (ε') and imaginary part (ε'') of complex permittivity were measured in the frequency range of 2-18 GHz ,and the results were shown in Fig. 7. ε' represents the storage ability of EM energy, while ε'' is connected with the energy dissipation and high ε'' indicates strong dielectric loss to EM wave. [27, 47] The complex permittivity of S4-1 is higher than those of other three samples (S1-1, S2-1 and S3-1) because of higher conductivity, but the complex permittivity of all these samples is not very high (less than 10) so that it is beneficial to the impedence match and could result in weak reflection and strong absorption.[17] The samples with 3D graphene structures have much higher ε'' than the corresponding samples with smashed TRGN. Moreover, these samples with TRGN present typical frequency dependent permittivity for both ε' and ε'' are found to decrease when frequency increases in the measured region, which may be related to a resonance behavior.[38] For example, as shown in Fig.7a and c, the values of ε' for S1-1 and S4-1 decrease from 3.73 and 8.72 to 1.64 and 4.40 while the values of ε'' decrease from 3.71 and 4.81 to 1.65 and 2.66 in the range of 2-18 GHz, respectively. The ε' and ε'' of the samples with smashed TRGN are almost unchanged with increasing frequency in 2-18 GHz (Fig. 7b and d). The ε' and ε'' of

S4-2 are higher than those of S1-2, S2-2 and S3-2 because of the higher filler loading of smashed TRGN. However, the ε'' of S4-2 is only around 0.5, which is much lower than the samples with TRGN. The loss tangent (tan $\delta_e = \varepsilon''/\varepsilon'$) indicates the inherent dissipation of EM energy for dielectric material, and higher values of tan δ_e mean more EM energy will be consumed. [24] As displayed in Fig. 7e and f, the values of the loss tangent(tan δ_e) of the samples with 3D graphene stuctures are higher than 0.43 in the range of 2-18 GHz, while the tan δ_e for samples with smashed TRGN are much lower, the highest loss tangent of S4-2 is less than 0.2. Thus, the samples with smashed TRGN should have much weaker EM wave absorption abilities than TRGN/ wax composites.

The reflection loss (RL) of a metal-backed single absorb layer was calculated as follows:

$$RL=20\log\frac{|Z_{in}-1|}{|Z_{in}+1|} \quad (1)$$

$$Z_{in}=\sqrt{\frac{\mu_r}{\varepsilon_r}}\tanh\left(j\frac{2\pi fd}{c}\sqrt{\mu_r\varepsilon_r}\right) \quad (2)$$

Where c is the light velocity, d represents the thickness of the absorbor, f means the microwave frequency, ε_r and μ_r are the complex relative permittivity and permeability, respectively.[48]

RL at a given sample thickness is expected to be as low as possible. The calculated RL curves of the composites with different thickness are shown in Fig. 8. The samples with TRGN show excellent EM wave absorption abilities. Fig. 8a-h exhibit the theoretical RL of the samples. S1-1 has the minimum RL of -44.06 dB at 8.28 GHz with a sample thickness of 5.0 mm, the bandwidth of RL below -10 dB is 4.9 GHz in the range of 6.55-11.45 GHz. The minimum RL of S2-1 at the thickness of

3.5 mm reaches -43.5 dB, and the effective bandwidth ranges from 9.36-16.83 GHz. The minimum RL of S3-1 and S4-1 can reach -43.6 dB at 3.5 mm and -42.4 dB at 3 mm. It is worth nothing that RL of S4-1 can reach -35.01 dB at only 2.5 mm with an effective bandwidth of 6.22 GHz (from 11.78 to18 GHz). As discussed before, the RL of the samples with smashed TRGN have much weaker abilities to absorb EM wave than TRGN/wax composites. It can be concluded that the unique 3D conductive network is an important reason for the enhanced EM wave absorption properties.

The strong EM wave absorbing capabilities of the TRGN/wax composites are attributed to electrical conduction loss, dielectric relaxation and multiple reflections. When EM waves propagated within the TRGN/wax composites, the directional motion of charge carriers on TRGN formed oscillatory current, thus, the conductive network within the wax could lead to high conduction loss.[23] The defects along with functional groups introduced into TRGN during wet and thermal treatment processes caused the dielectric relaxation. Firstly, defects acting as polarization centers would generate polarization relaxation under the altering electromagnetic field and attenuate EM wave, resulting in a profound effect on the loss of EM wave. Secondly, there are redidual oxygen containing chemical bonds in RGO. The different abilities to catch electrons between carbon atom and oxygen atom lead to electronic dipole polarization. Hence, the TRGN/wax composites would have better EM wave absorbing abilities through the electron motion hysteresis.[28, 49] Furthermore, The 2D structure and high aspect ratio of RGO in TRGN/wax composites are benefit for the multiple reflections.[23, 50] The absorbed energy is dissipated as heat when TRGN/wax composite is irradiated by EM waves,[23, 51] as shown in Fig. 9. For the samples with smashed TRGN, the conductive network can hardly be established due to the very low filler loadings and the aggregation of smashed TRGN.

Table1 shows the typical graphene-based composites and their corresponding EM wave absorbing performance. It is find that the composites with bare RGO require much lower filler loadings than RGO hybrid structures,[23, 26, 30, 32, 50] and the effective filler loadings in the TRGN/wax composites (~0.5 wt%, ~1 wt%, ~1.5 wt% and ~2 wt%) in our work are lower than these reported composites with bare RGO.[23, 24, 32] Furthermore, the effective bandwidth of S2-1 is broader than the composites with much higher filler loadings (>25 wt%) in previous studies.[4, 23, 28-30] The performance of TRGN-based composites are also very competitive to the composites with bare RGO at low loading (<5 wt%).[23, 24]

By using 3D ultralight TRGN as an unique integrated graphene filler rather than dispersing RGO into matrix, we can prevent RGO sheets from aggregation, so that the effective conductive interconnections could form at relatively lower loading. Thus, the 3D TRGN should be an ideal candidate for EM wave absorbing.

4. Conclusions

In summary, we have synthesized ultralight 3D porous graphene networks and demonstrated the EM wave absorption performances of the wax-based composites with the 3D conductive graphene structures. The composites have presented strong EM wave absorption abilities and wide absorption bandwidths at very low graphene loadings (~0.5, ~1, ~1.5 and ~2 wt%). Compared to the magnetic/conductive hybrids which were obtained by conventional approaches, the concept of achieving 3D porous structures highlights great potential in the development of EM wave-absorbing composites at very low filler loadings..

Acknowledgments

This work is supported by the Natural Science Foundation of China (No. 51373096) and CAST Foundation (No. 201233). Instrumental Analysis Center of Shanghai Jiao Tong University and National Engineering Research Center for Nanotechnology are gratefully acknowledged for assisting relevant analyses.

References

1. J. Liu, R. Che, H. Chen, F. Zhang, F. Xia, Q. Wu and M. Wang, *Small*, 2012, **8**, 1214-1221.
2. D. Chen, G. S. Wang, S. He, J. Liu, L. Guo and M. S. Cao, *J. Mater. Chem. A*, 2013, **1**, 5996-6003.
3. G. S. Wang, S. He, X. Luo, B. Wen, M.-M. Lu, L. Guo and M. S. Cao, *RSC Adv.*, 2013, **3**, 18009-18015.
4. X. Sun, J. He, G. Li, J. Tang, T. Wang, Y. Guo and H. Xue, *J. Mater. Chem. C*, 2013, **1**, 765-777.
5. Y. Z. Wei, G. S. Wang, Y. Wu, Y. H. Yue, J. T. Wu, C. Lu and L. Guo, *J. Mater. Chem. A*, 2014, **2**, 5516-5524.
6. Q. Wang, Z. Lei, Y. Chen, Q. Ouyang, P. Gao, L. Qi, C. Zhu and J. Zhang, *J. Mater. Chem. A*, 2013, **1**, 11795-11801.
7. G. S. Wang, X. J. Zhang, Y.-Z. Wei, S. He, L. Guo and M. S. Cao, *J. Mater. Chem. A*, 2013, **1**, 7031-7036.
8. G. S. Wang, Y. Y. Wu, X. J. Zhang, Y. Li, L. Guo and M. S. Cao, *J. Mater. Chem. A*, 2014, **2**, 8644-8651.
9. S. He, G. S. Wang, C. Lu, J. Liu, B. Wen, H. Liu, L. Guo and M. S. Cao, *J. Mater. Chem. A*, 2013, **1**, 4685-4692.
10. Y. Deng, L. Zhao, B. Shen, L. Liu and W. Hu, *J. Appl. Phys.*, 2006, **100**, 014304.
11. X. M. Meng, X. J. Zhang, C. Lu, Y. F. Pan and G. S. Wang, *J. Mater. Chem. A*, 2014, **2**, 18725-18730.
12. C. L. Zhu, M. L. Zhang, Y. J. Qiao, Xiao.G., F. Zhang and Y. J. Chen, *J Phys Chem C*, 2010, **114**, 16229-16235.
13. M. M. Lu, W. Q. Cao, H. L. Shi, X. Y. Fang, J. Yang, Z. L. Hou, H. B. Jin, W. Z. Wang, J. Yuan and M. S. Cao, *J. Mater. Chem. A*, 2014, **2**, 10540-10547.
14. X. Liu, Z. Zhang and Y. Wu, *Compos Part B-Eng.*, 2011, **42**, 326-329.
15. A. Wadhawan, D. Garrett and J. M. Perez, *Appl. Phys. Lett.*, 2003, **83**,

2683-2685.
16. F. Schedin, A. K. Geim, S. V. Morozov, E. W. Hill, P. Blake, M. I. Katsnelson and K. S. Novoselov, *Nat. mater.*, 2007, **6**, 652-655.
17. C. Wang, X. Han, P. Xu, X. Zhang, Y. Du, S. Hu, J. Wang and X. Wang, *Appl. Phys. Lett.*, 2011, **98**, 072906.
18. H. Yu, T. Wang, B. Wen, M. Lu, Z. Xu, C. Zhu, Y. Chen, X. Xue, C. Sun and M. Cao, *J. Mater. Chem.*, 2012, **22**, 21679-21685.
19. Y. Ren, C. Zhu, L. Qi, H. Gao and Y. Chen, *RSC Adv.*, 2014, **4**, 21510-21516.
20. I. K. Moon, J. Lee, R. S. Ruoff and H. Lee, *Nat. commun.*, 2010, **1**, 73.
21. R. Larciprete, S. Fabris, T. Sun, P. Lacovig, A. Baraldi and S. Lizzit, *J. Am. Chem. Soc*, 2011, **133**, 17315-17321.
22. M. U. Okan Oner Ekiz, H. Guner, A. Koray Mizrak and A. Dana, *ACS Nano*, 2011, **3**, 2475-2482.
23. X. Bai, Y. Zhai and Y. Zhang, *J. Phys. Chem. C*, 2011, **115**, 11673-11677.
24. V. K. Singh, A. Shukla, M. K. Patra, L. Saini, R. K. Jani, S. R. Vadera and N. Kumar, *Carbon*, 2012, **50**, 2202-2208.
25. X. J. Zhang, G. S. Wang, W. Q. Cao, Y. Z. Wei, M. S. Cao and L. Guo, *RSC Adv.*, 2014, **4**, 19594-19601.
26. T. Chen, F. Deng, J. Zhu, C. Chen, G. Sun, S. Ma and X. Yang, *J. Mater. Chem.*, 2012, **22**, 15190-15197.
27. X. J. Zhang, G. S. Wang, W. Q. Cao, Y. Z. Wei, J. F. Liang, L. Guo and M. S. Cao, *ACS Appl. Mater. Interfaces*, 2014, **6**, 7471-7478.
28. L. Wang, Y. Huang, X. Ding, P. Liu and M. Zong, *RSC Adv.*, 2013, **3**, 23290-23295.
29. H. L. Xu, H. Bi and R. B. Yang, *J. Appl. Phys.*, 2012, **111**, 07A522.
30. M. Han, X. Yin, L. Kong, M. Li, W. Duan, L. Zhang and L. Cheng, *J. Mater. Chem. A*, 2014, **2**, 16403-16409.
31. W. L. Song, M. S. Cao, L. Z. Fan, M. M. Lu, Y. Li, C. Y. Wang and H. F. Ju, *Carbon*, 2014, **77**, 130-142.
32. L. Kong, X. Yin, X. Yuan, Y. Zhang, X. Liu, L. Cheng and L. Zhang, *Carbon*, 2014, **73**, 185-193.
33. M. A. Worsley, T. Y. Olson, J. R. I. Lee, T. M. Willey, M. H. Nielsen, S. K. Roberts, P. J. Pauzauskie, J. Biener, J. H. Satcher and T. F. Baumann, *J. Phys. Chem. Lett.*, 2011, **2**, 921-925.
34. X. Zhang, Z. Sui, B. Xu, S. Yue, Y. Luo, W. Zhan and B. Liu, *J. Mater. Chem.*, 2011, **21**, 6494-6497.
35. H. Sun, Z. Xu and C. Gao, *Adv. Mater.*, 2013, **25**, 2554-2560.
36. L. Qiu, D. Liu, Y. Wang, C. Cheng, K. Zhou, J. Ding, V. T. Truong and D. Li, *Adv mater*, 2014, **26**, 3333-3337.
37. H. Hu, Z. Zhao, W. Wan, Y. Gogotsi and J. Qiu, *Adv mater*, 2013, **25**, 2219-2223.
38. H. Zhang, A. Xie, C. Wang, H. Wang, Y. Shen and X. Tian, *RSC Adv*, 2014, **4**, 14441-14446.
39. H. Zhang, A. Xie, C. Wang, H. Wang, Y. Shen and X. Tian, *J. Mater. Chem. A*,

2013, **1**, 8547-8552.
40. S. Stankovich, D. A. Dikin, R. D. Piner, K. A. Kohlhaas, A. Kleinhammes, Y. Jia, Y. Wu, S. T. Nguyen and R. S. Ruoff, *Carbon*, 2007, **45**, 1558-1565.
41. J. Liang, Y. Huang, L. Zhang, Y. Wang, Y. Ma, T. Guo and Y. Chen, *Adv. Funct. Mater*, 2009, **19**, 2297-2302.
42. L. Liu, A. Baeber, S. Nuriel and H. Wagner, *Adv. Funct. Mater.*, 2005, **15**, 975-980.
43. Z. G. Wang, X. T. Zu, S. Zhu, X. Xiang, L. M. Fang and L. M. Wang, *Phys. Lett. A*, 2006, **350**, 252-257.
44. O. C. Compton, D. A. Dikin, K. W. Putz, L. C. Brinson and S. T. Nguyen, *Adv.mater.*, 2010, **22**, 892-896.
45. A. Gupta, G. Chen, P. Joshi, S. Tadigadapa and P. C. Eklund, *Nano Lett.*, 2006, **6**, 2667-2673.
46. P. Hasin, M. Alpuche-Aviles and Y. Wu, *J. Phys. Chem. C*, 2010, 114, 16229-16235.
47. D. Micheli, C. Apollo, R. Pastore and M. Marchetti, *Compos. Sci. Technol.*, 2010, **70**, 400–409.
48. H. Zhang, C. Zhu, Y. Chen and H. Gao, *Chemphyschem.*, 2014, **15**, 2261-2266.
49. T. Wang, Z. Liu, M. Lu, B. Wen, Q. Ouyang, Y. Chen, C. Zhu, P. Gao, C. Li, M. Cao and L. Qi, *J. Appl. Phys.*, 2013, **113**, 024314.
50. Z. Chen, C. Xu, C. Ma, W. Ren and H. M. Cheng, *Adv. Mater.*, 2013, **25**, 1296-1300.
51. Y. Ren, C. Zhu, S. Zhang, C. Li, Y. Chen, P. Gao, P. Yang and Q. Ouyang, *Nanoscale*, 2013, **5**, 12296-12303.

Figure Captions:

Fig. 1 The schematic for the formation process of TRGN and TRGN/wax composite.

Fig. 2 (a) XRD patterns and (b) Raman spectra of GO and TRGN-1.

Fig. 3 TGA of (a) PVA and (b) GO/PVA network.

Fig. 4 XPS spectra of (a) GO and (b) TRGN-1.

Fig. 5 SEM images of (a,b) TRGN-1; photo images of (c) TRGN-1/wax composite, (d) burning the TRGN-1/wax composite and (e) the network after the wax was burnt out; (f) SEM image of the network after the wax was burnt out.

Fig. 6 Photo images and SEM images of (a) S1-1 (TRGN/wax) and (b) S2-1 (smashed-TRGN /wax).

Fig. 7 Electromagnetic characteristics of the samples in the 2-18 GHz: real permittivity of (a) TRGN/wax composites and (b) smashed-TRGN/wax composite; imaginary permittivity of (c) TRGN/wax composites and (d) smashed-TRGN/wax composite; loss tangent of (e) TRGN/wax composites and (f) smashed-TRGN/wax composite.

Fig. 8 Reflection loss curves for the TRGN/wax samples with different thickness in the frequency of 2-18 GHz: (a) S1-1, (b) S1-2, (c) S2-1, (d) S2-2, (e) S3-1, (f) S3-2, (g) S4-1 and (h) S4-2.

Fig. 9 Schematic illustration of the dissipation route of EM wave in the TRGN/wax composite.

Fig.1

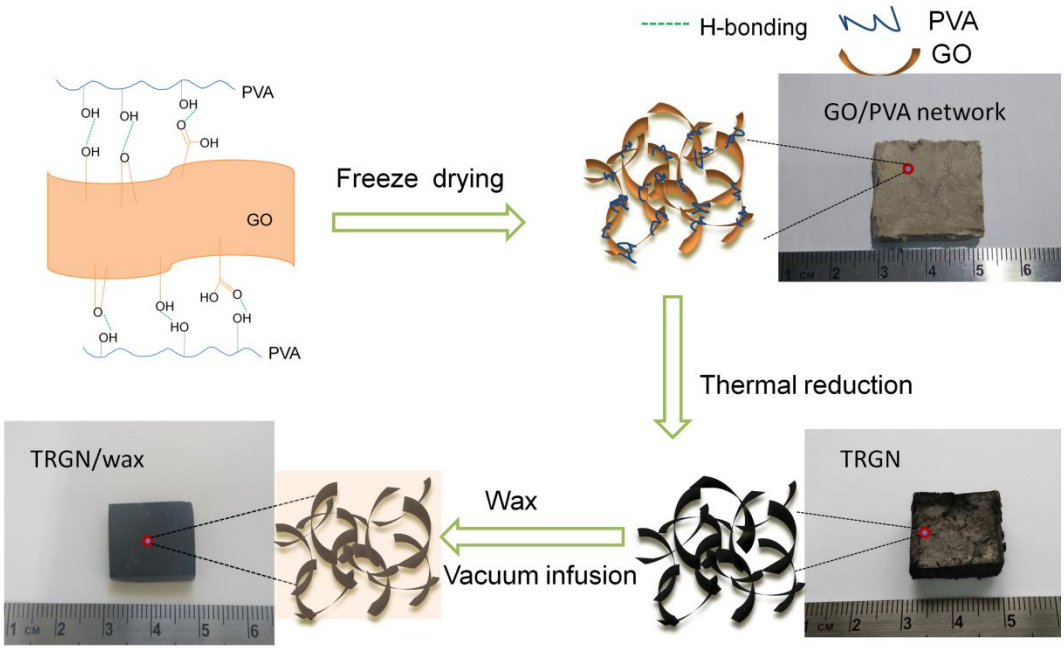

Fig. 2

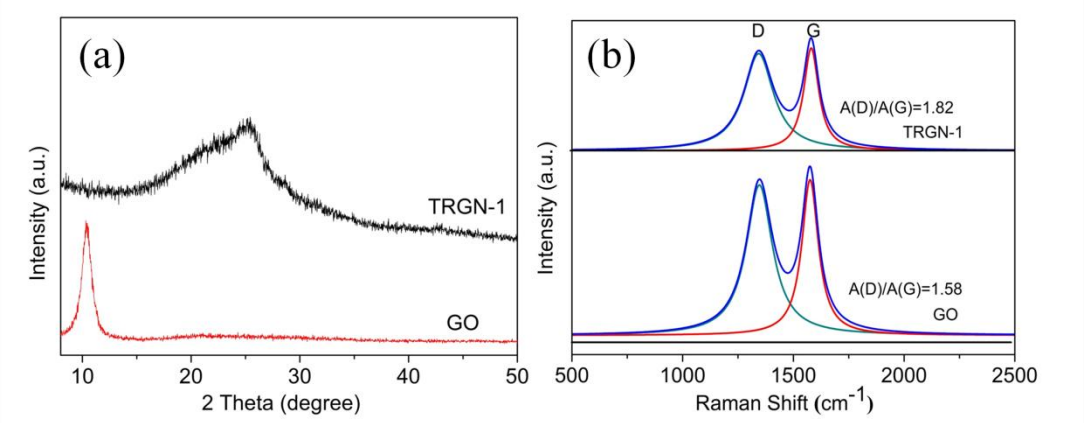

Fig. 3

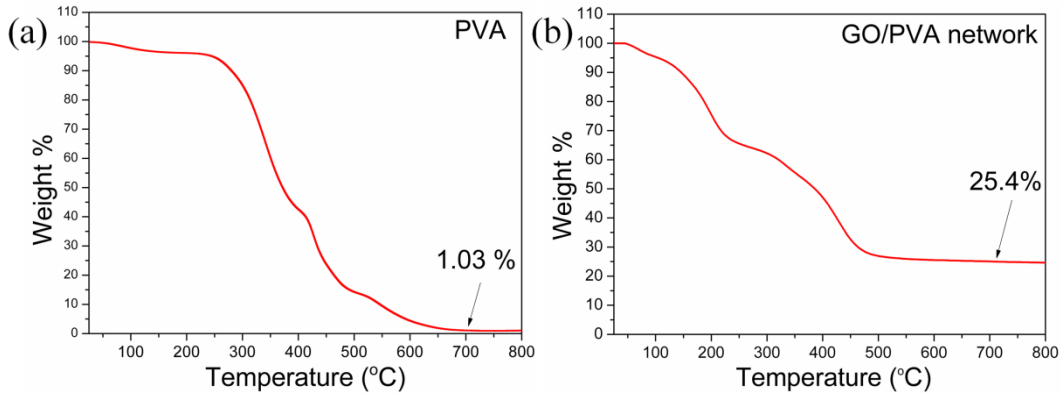

Fig. 4

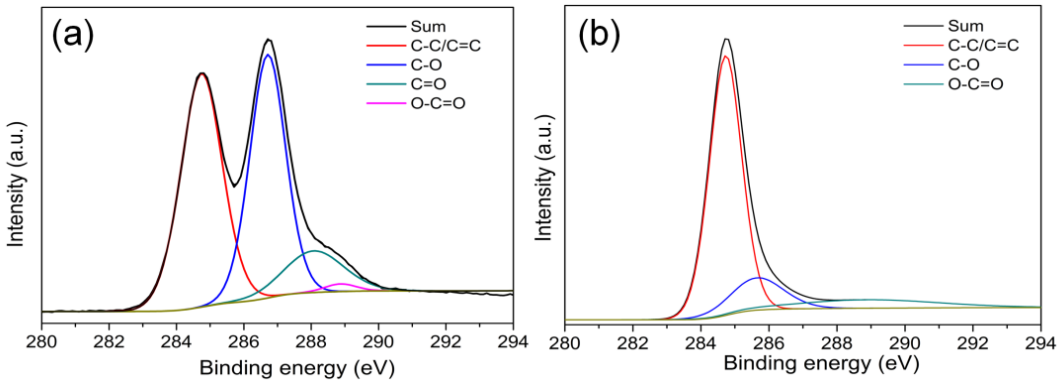

Fig. 5

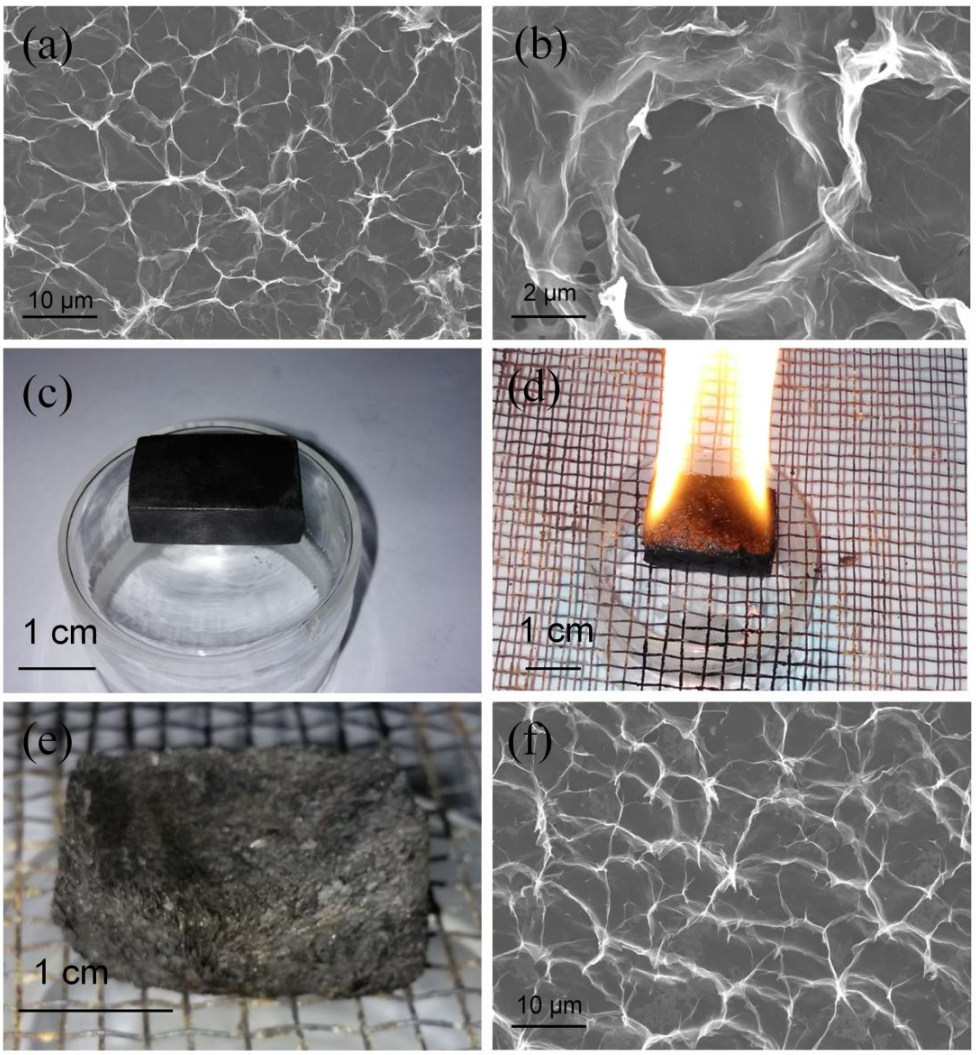

Fig. 6

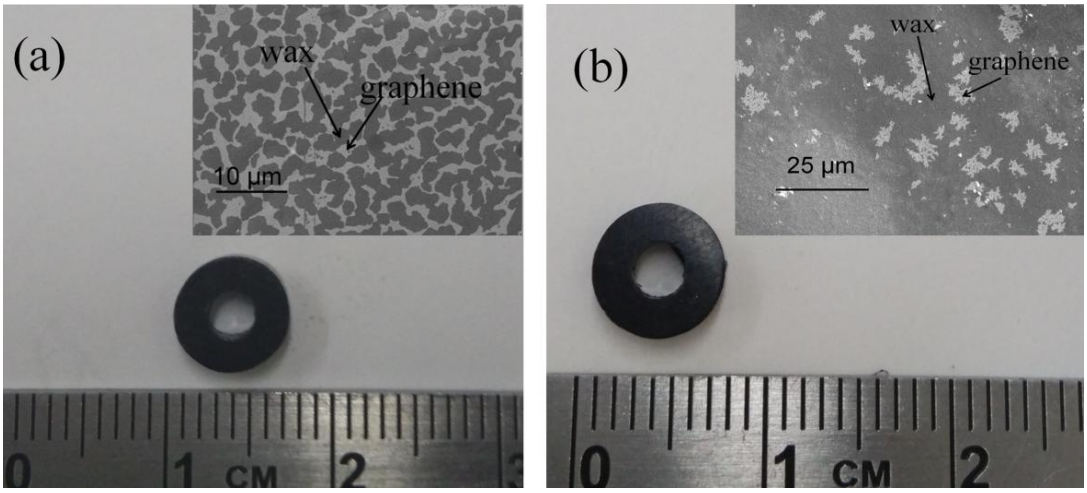

Fig. 7

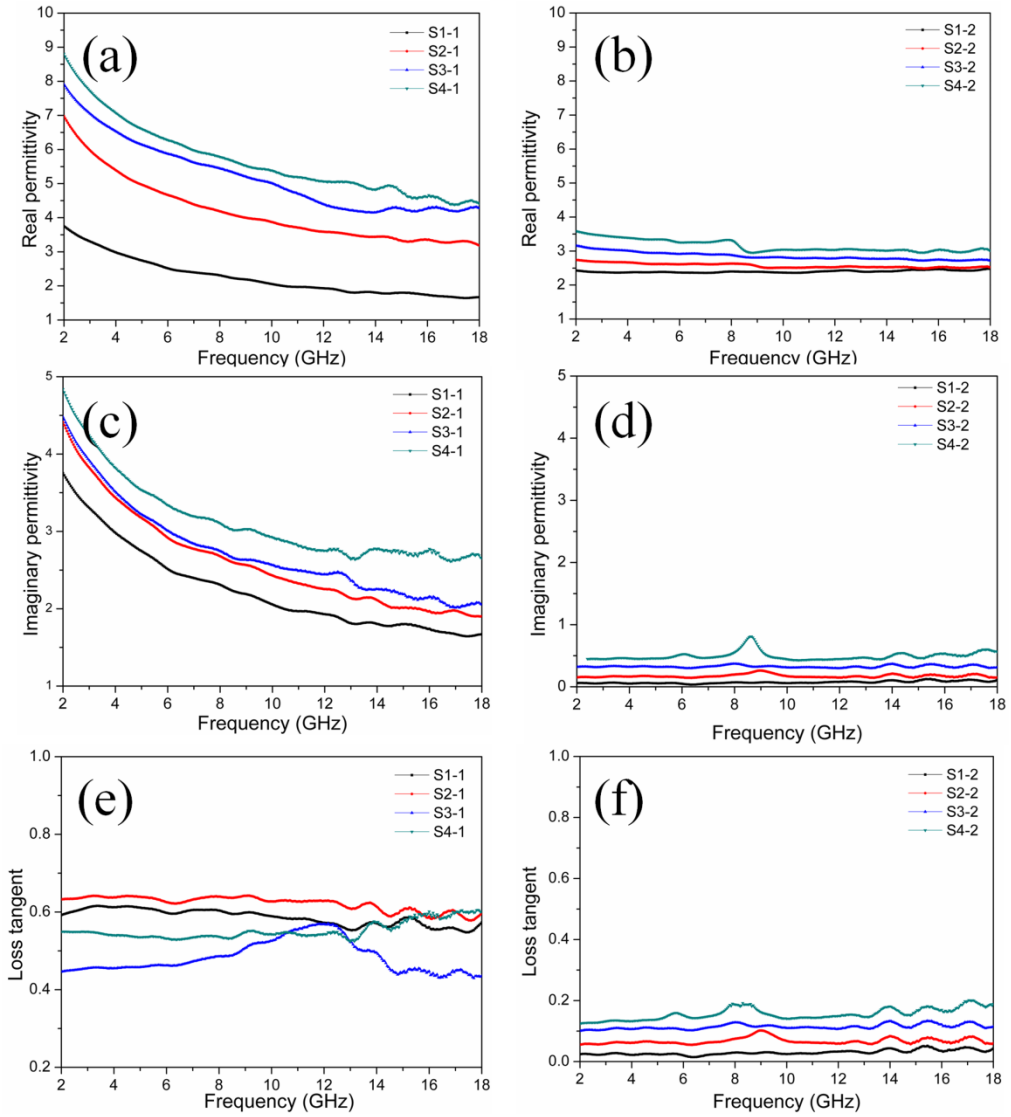

Fig. 8

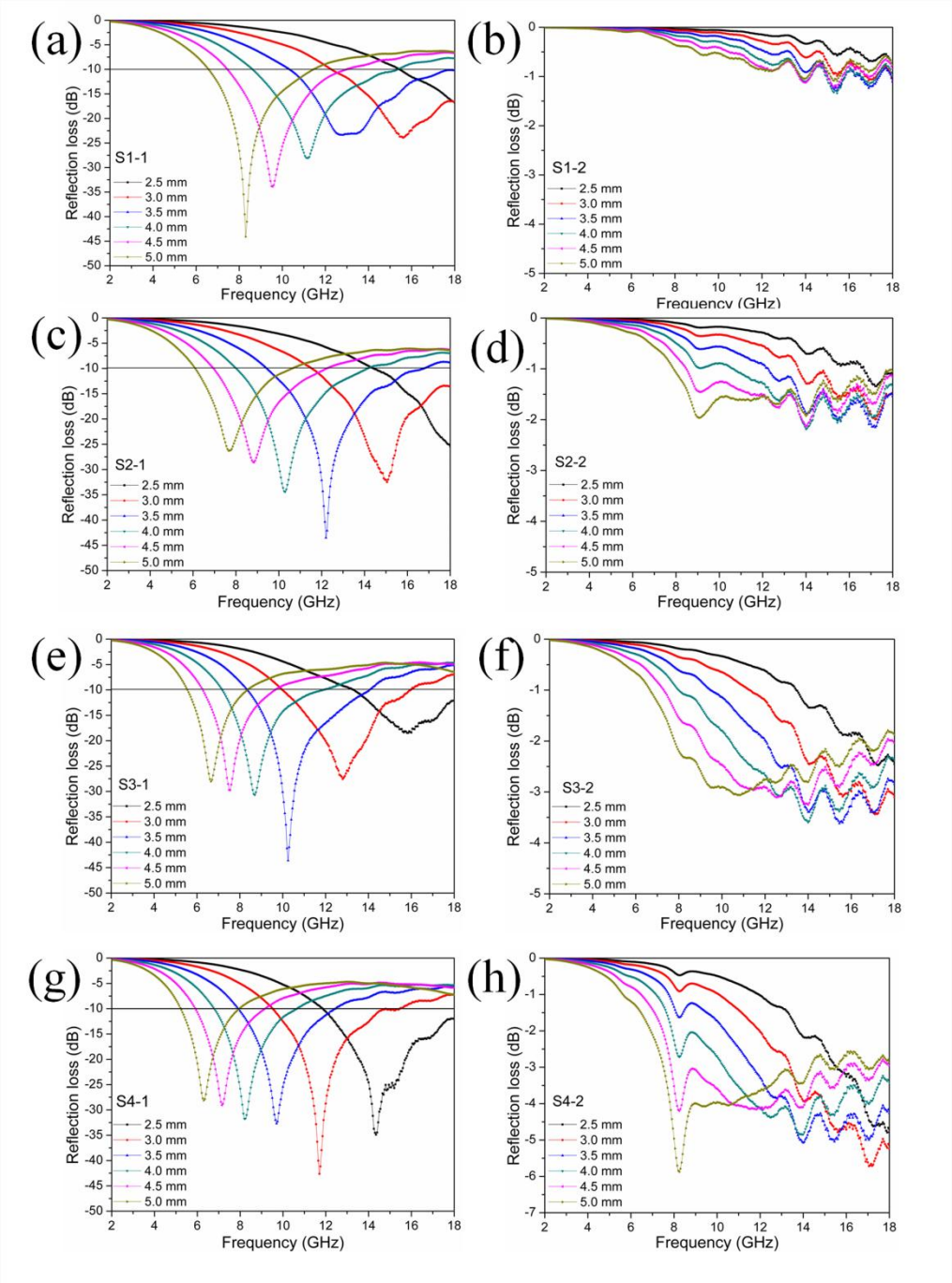

Fig. 9

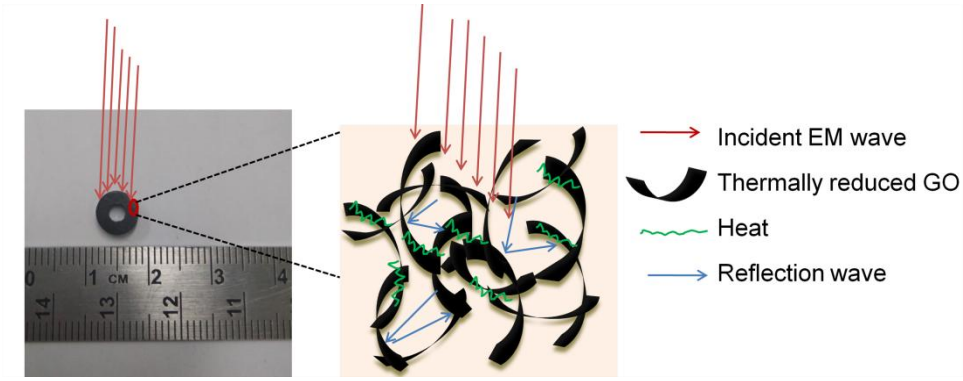

Table Captions

Table 1 Typical carbon based composites for EM wave absorption reported in literature. (PU:polyurethane; PDMS: poly(dimethyl siloxane); PEO:poly (ethylene oxide); NBR:nitrile butadiene rubber)

Table 1

Filler	Matrix	Filler loading	Minimum RL (dB)	Thickness (mm)	Effective bandwidth (<-10dB)(GHz)	Frequency range(<-10dB) (GHz)	Refs
TRGN-1	Wax	~0.5 wt%	-44.06	5	4.9	6.55-11.45	This work
TRGN-2	Wax	~1 wt%	-44.5	3.5	7.47	9.36-16.83	This work
TRGN-3	Wax	~1.5 wt%	-43.6	3.5	5.8	8.2-14.12	This work
TRGN-4	Wax	~2 wt%	-42.4	3	6.14	9.44-15.58	This work
RGO	PEO	1 wt%	-16	5	2.5	6-8.5	23
RGO	PEO	5 wt%	-38.8	1.8	4.1	13.9-18	23
CNT/RGO	PDMS	5 wt%	-55	2.75	3.5	8.5-12	29
RGO	NBR	2 wt%	>-10	4	-	-	24
RGO	NBR	10 wt%	-43.9	4	5.8	9.2-15	24
RGO/α-Fe_2O_3	Wax	8 wt%	-33.5	3	6.4	10.8-17.2	36
RGO /NiO/SiO_2	Wax	25 wt%	-57	3	4	8-12	26
RGO/ Fe_3O_4	Wax	30 wt%	-24	2	4.9	10.8-15.7	27
RGO/Fe_3O_4	Wax	40 wt%	-27	4	2	4.5-6.5	4
RGO/ZnO	Wax	50 wt%	-45.05	2.2	3.3	8.8-12.1	28
RGO/Ni	Wax	60 wt%	-17	5	3	3.0-4.0,12.0-14.0	24